scientific reports

Check for updates

OPEN

Exploring the molecular interaction of mebendazole with bovine serum albumin using multi-spectroscopic approaches and molecular docking

Reem N. El Gammal[1]✉, Heba Elmansi[2], Ali A. El-Emam[1], Fathalla Belal[2] & Mohammed E. A. Hammouda[1,3]

This article presents the binding interaction between mebendazole (MBZ) and bovine serum albumin. The interaction has been studied using different techniques, such as fluorescence quenching spectroscopy, UV–visible spectroscopy, synchronous fluorescence spectroscopy, fourier transform infrared, and fluorescence resonance energy transfer in addition to molecular docking. Results from Stern Volmer equation stated that the quenching for MBZ-BSA binding was static. The fluorescence quenching spectroscopic study was performed at three temperature settings. The binding constant (k_q), the number of binding sites (n), thermodynamic parameters (ΔH°, ΔS° and ΔG°), and binding forces were determined. The results exhibited that the interaction was endothermic. It was revealed that intermolecular hydrophobic forces led to the stabilization of the drug-protein system. Using the site marker technique, the binding between MBZ and BSA was found to be located at subdomain IIA (site I). This was furtherly approved using the molecular docking technique with the most stable MBZ configuration. This research may aid in understanding the pharmacokinetics and toxicity of MBZ and give fundamental data for its safe usage to avoid its toxicity.

Serum albumin is the main blood plasma protein that forms molecular interactions with small molecules through binding at specific sites and assisting in their transport throughout the circulation, either exogenously or endogenously[1]. Moreover, the structural similarities between bovine serum albumin (BSA) and human serum albumin (HSA) make it an essential subject in in-vitro research. BSA is composed of 583 amino acids with a molecular weight of 66.5 kDa. The protein structure of BSA is divided into three homologous subdomains that are assembled in a linear arrangement and subdivided into subdomains A and B[2–4]. BSA contains two tryptophan residues and 20 tyrosin residues. Ligands may bind to BSA at more than one site, which are situated in the hydrophobic cavities of subdomains IIA or IIIA. Because of high structural similarity with HSA, properties such as low cost, easy availability, and similarity in ligand binding patterns with HSA have led to the using of BSA as a model protein for studying the interactions between drugs and plasma proteins. The stable BSA-drug complex is the perfect model for obtaining basic insights into plasma-drug binding[5].

The pharmacokinetics of a drug is mainly dependent on the nature of its interaction with plasma proteins, especially albumins[6,7]. It was found that the drug's affinity to serum albumin basically controls its concentrations in the free and bound forms, however their equilibrium is critical to the drug's mode of action. Consequently, it is crucial to reach a full understanding of the drug's binding mechanism with serum albumin to avoid its toxic effects[8].

Mebendazole (MBZ) is a benzimidazole carbamate derivative (Fig. 1). It is highly lipophilic (log P 2.83) with low solubility. It undergoes extensive first-pass metabolism[9]. MBZ is poorly absorbed from the gastrointestinal tract; it is used orally to treat intestinal nematode infections such as ascariasis, enterobiasis, hookworm, and trichuriasis[9]. It inhibits or destroys cytoplasmic microtubules in the worm's intestinal or absorptive cells. Besides, it acts through inhibition of glucose uptake and depletion of glycogen stores leading to worm's death within several days[9]. Mebendazole is a novel cancer medicine focusing on cells that are resistant to existing treatments.

[1]Department of Medicinal Chemistry, Faculty of Pharmacy, Mansoura University, Mansoura 35516, Egypt. [2]Pharmaceutical Analytical Chemistry Department, Faculty of Pharmacy, Mansoura University, Mansoura 35516, Egypt. [3]Department of Pharmaceutical Chemistry, Faculty of Pharmacy, Horus University - Egypt (HUE), New Damietta, Egypt. ✉email: reemnashaat@std.mans.edu.eg

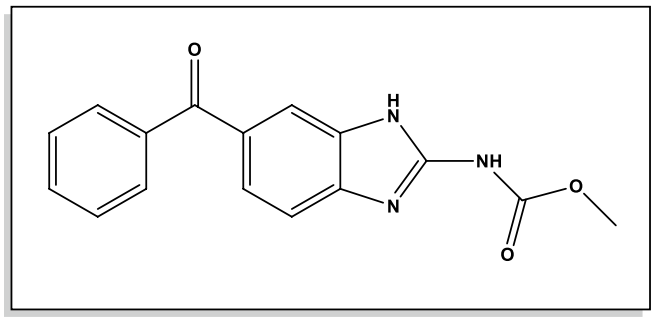

Figure 1. Structural formula of Mebendazole (MBZ).

It exhibits cytotoxic activity, which synergizes with ionizing radiations and different chemotherapeutic agents and stimulates an antitumoral immune response[10].

In the case of mebendazole overdose, it exerts acute oral toxicity, and its LD_{50} is 620 mg/kg. Symptoms of overdose include elevated liver enzymes, headaches, hair loss, low levels of white blood cells (neutropenia), fever, and itching[11]. It is evident that it seems very important to study the drug's binding mechanism with serum albumin to avoid its toxic effects.

In this in-vitro study, the interaction between MBZ and BSA has been studied using the quenching fluorescence method. Thermodynamic parameters were computed to obtain binding constants at various temperature settings using Tris–HCl (pH 7.4). As well, the binding forces and the binding sites were determined. UV–visible spectroscopy, synchronous fluorescence (SF), and FTIR were used to investigate changes in protein structure. The interaction was indicated to be endothermic. Using the site marker technique, the binding between MBZ and BSA was found to be located at subdomain IIA (site I). This was also confirmed using molecular docking technique with the most stable MBZ configuration. So, these results proved the binding relationship between MBZ and BSA, suggesting recommendations for further studies and researches.

Experimental

Materials and chemicals.

- Mebendazole (MBZ) was kindly provided by Alexandria Co. for Pharmaceuticals and Chemical Industries, Alexandria, Egypt
- Diazepam was kindly provided by Amoun Pharmaceutical Co., Cairo, Egypt.
- Indomethacin was received as a gift from Medical Union Pharmaceuticals Co, Ismailia, Egypt.
- Analytical grade Tris (hydroxymethyl) aminomethane hydrochloride (Tris–HCl) was bought from Sigma Aldrich (Germany).
- Bovine serum albumin (BSA) was also bought from Sigma Aldrich Co. (Chemie Gmbh, Munich, Germany), with batch No. SLBM6044V.

Equipment and software. *For Fluorescence measurements.* Cary Eclipse Fluorescence Spectrophotometer was employes with Xenon flash lamp from Agilent Technologies (USA). A high voltage mode was used (900 V); the slit width was 5 nm and the smoothing factor was 20. Data were processed using prism.

When measuring the fluorescence spectrum, it is widely assumed that the inner filter effect (IFE) must be detected[12]. The following equation was used for correcting the fluorescence intensity with MBZ:

$$F_{cor} = F_{obs} \times e^{(A_{ex}+A_{em})/2}$$

F_{cor}: the corrected fluorescence intensity and, F_{obs} observed fluorescence intensity in the experiment. A^{ex} and A^{em} form the summation of MBZ absorbance at excitation 285 nm and the emission wavelength (λ), respectively.

A Hanna pH-meter (Romania) was used for adjusting pH.

UV–visible measurements. An operation of Shimadzu (Kyoto, Japan) UV-1601 PC using quartz cuvette, UV–visible double-beam spectrophotometer on a fast scan speed was conducted.

Infrared spectroscopy. FT-IR spectra are recorded using Thermo Fisher Scientific (168 Third Avenue Waltham, MA USA) on a Thermo Fisher Scientific Nicolet—iS10 FT-IR Spectrometer. It was equipped with a Ge/KBr beam splitter and a DTGS detector from 4000 to 1000 cm^{-1}. For all measurements, 32 scans were recorded at 4 cm^{-1} resolution.

Molecular docking software. Downloading the crystal structure (3D) of BSA was made from the Protein Data Bank (www.rcsb.org), Code 4F5S[13,14], and it was added into the Molecular Operating Environment software

package (MOE 2019). This was conducted for pre-optimization by excluding water molecules and heteroatoms and adding the hydrogen atoms. ChemDraw Ultra 17.1 was used for obtaining the 3D structure of MBZ, and MOE 2019 software package in the compatible file format was used for acquiring the minimized energy structure and geometries of MBZ. A determination of binding pocket on BSA was detected. Keeping the receptor rigid, the triangle matcher principle was employed for the placement phase and the London dG function was employed for scoring using 30 runs for the drug.

General procedure

Preparation of stock solutions. BSA (2000 μM) stock solution was freshly prepared in bidistilled water. MBZ stock solution (100 μM) was prepared in formic acid. Tris hydrochloride buffer solution (pH = 7.4) was prepared in concentration of 20.0 mM in bidistilled water. All stock solutions were refrigerated at 4 °C and further diluted if necessary to get the working solutions.

UV–visible absorption method. In this method, BSA concentration was kept constant at 40 μM, whereas the concentration of the drug was changed from 1 to 15 μM. At a temperature of 298 K, the UV region of 190–350 nm was scanned. The volume of solutions was completed using Tris buffer (20 mM, pH 7.4). To eliminate interference, the spectra were adjusted by subtracting the solvent absorption from both BSA and BSA-MBZ complex absorptions spectra.

Fluorescence quenching method. BSA fluorescence quenching was studied at three temperatures: 298, 310, and 318 K along wavelength (300–500 nm) after excitation at 285 nm. BSA concentration was remained constant at 40 μM, while MBZ concentration was increased from 4 to 45 μM (4, 5, 10, 15, 20, 25, 30, 35, 40, 45 μM).

Synchronous fluorescence method. BSA synchronous fluorescence spectra were scanned in the 200–320 nm range with different concentrations of MBZ (0–45 μM) after adjustment of Δλ at 60 nm for tryptophan and Δλ at 15 nm for tyrosine residues.

FTIR method. Recording of FTIR spectra of BSA (500 μM) with and without MBZ was accomplished over the range of 1500–1800 cm^{-1} and setting BSA with the drug molar ratio at 1:1. Meanwhile, the value of absorbance of buffer and free MBZ solutions were measured and digitally subtracted from the spectra of the BSA-MBZ complex.

Site probe studies. The competitive binding approaches were developed by using two approved site markers that are specific to the two main sites (Indomethacin for site I and diazepam for site II). The experiment was established by mixing equal concentrations of BSA and site marker, then setting them aside for 30 min to ensure maximal binding. Afterward, the mixture was titrated with different concentrations of MBZ, and the fluorescence emission spectra were recorded.

Results and discussion

A detailed analysis of interactions between MBZ with BSA is not available in the literature. This tempted us to extensively characterize the interactions of MBZ with BSA using various spectroscopic approaches. The findings in this study indicate that MBZ binds with BSA at the site I. Thermodynamic investigations revealed that a stable ground state complex was formed between MBZ and BSA. The static mode of quenching was predominantly involved in the interaction of these two molecules. FTIR analysis confirmed that the binding of MBZ induced conformational changes in both the secondary and tertiary structure of BSA. Collectively, this paper characterizes the biochemical interactions occurring between BSA and MBZ and provides a comprehensive understanding of the pharmacodynamic properties of MBZ at the molecular level.

UV–visible spectrophotometry. It is a reliable approach that may be used to investigate protein structural changes and the formation of protein-drug complexes[15,16]. The protein spectrum is susceptible to the microenvironment surrounding the chromophores[17]. Figures 2a,b show the influence of MBZ on the spectra of BSA. As illustrated in Fig. 2a, there is a detectable high absorption peak at 270 nm. While Fig. 2b reveals an increase in peak intensity with increasing MBZ concentrations confirming the interaction between MBZ and BSA.

Fluorescence spectroscopy. Fluorescence spectroscopy is utilized to investigate drug-protein binding mechanisms to get information on the binding constant, number of binding sites, and thermodynamic parameters. Basically, changes in protein fluorescence intensity are detected at the maximum emission wavelength[12,18]. Adding MBZ to the BSA solution causes the formation of the MBZ-BSA, complex as shown in Fig. 3A–C. BSA fluorescence emission is quenched with increasing MBZ concentrations. It has two tryptophan residues and 18 tyrosine residues that display a strong bond upon protein excitation at 285 nm[19].

Quenching of FI under these conditions is concentration-dependent and could be defined by the Stern–Volmer equation. The equation is adopted to evaluate the binding parameters at various temperatures:

$$\frac{F_o}{F} = 1 + K_{sv}[Q] \quad (1)$$

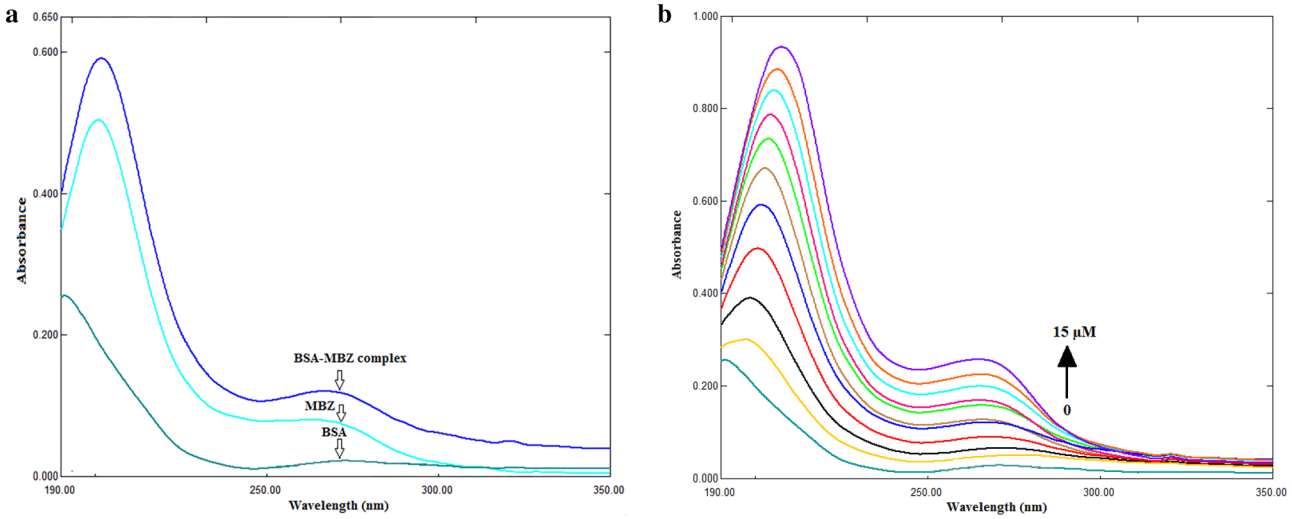

Figure 2. (**a**) UV–visible absorption spectra of MBZ (5 µM), BSA (40 µM), and BSA-MBZ complex at 298 K and pH 7.4. (**b**) UV–visible absorption spectra of BSA (C_{BSA} = 40 µM) and MBZ C_{MBZ} = (1, 2, 4, 5, 6, 8, 9, 10, 12, 15 µM) at 298 K and pH 7.4.

F_o and F: fluorescence intensities of BSA before and after binding with (MBZ). K_{SV} is the Stern–Volmer constant and [Q] is the concentration of the quencher.

The plot of Eq. (1) in Fig. 4 was used to calculate the Stern–Volmer constant. Fluorescence quenching can be managed using one of three mechanisms: dynamic, static, and combination of the two mechanisms, but the principles of the two procedures vary since they are temperature-dependent[12,20]. The quenching constants in the dynamic quenching mechanism are predicted to increase along with rising temperatures, resulting in large diffusion coefficients. However, higher temperatures can cause a loss in complex stability, which can cause a decrease in the quenching constant value for static quenching[21]. Complex formation is proved by quenching rate constant (k_q) values. The following equation is used for their calculation:

$$k_q = \frac{K_{sv}}{\tau o} \tag{2}$$

where k_q is the bimolecular quenching rate constant, τ_0 *is* the average lifetime of the fluorophore in the excited state that is for a biomacromolecule 10^{-8} s[12,22,23].

Figure 4 represents Stern–Volmer graphs at various temperature settings for MBZ quenching of BSA fluorescence, whereas Table 1 gives the K_{SV} and k_q values. The order of magnitude of the quenching rate constant k_q in this study was found to be 10^{12}. Furthermore, the value of the bimolecular quenching rate constant was calculated and was found to be more than 2×10^{10} L mol^{-1} s^{-1}[24], suggesting a static quenching of the interaction between MBZ and BSA[25,26].

Estimation of the binding constant and number of binding sites. Both were determined using the so called Modified Stern–Volmer equaton[27]:

$$\log \frac{F_o - F}{F} = \log K_b + n \log [Q] \tag{3}$$

where K_b and n are the binding constant and number of the binding site, respectively. Both can be obtained by plotting $\log\left(\frac{F_o - F}{F}\right)$ against log [Q]. The values of log K_b and n are provided by the intercept and slope of Fig. 5, respectively. Table 2 shows the results attained at various temperature settings. The binding ratio of BSA to MBZ was found to be nearly 1:1, and the binding constant decreases upon increasing temperature.

Determination of thermodynamic parameters. The drug-protein binding involves four main forces, viz: hydrophobic forces, hydrogen bonding, electrostatic interactions, and van der Waals forces. The thermodynamic parameters, including enthalpy change (ΔH^o) and entropy change (ΔS^o) describe the binding forces in the process[28]. Ross and Subramanian investigated the relationship between changes in thermodynamic parameter values and binding forces[29]. When $\Delta H^o > 0$ and $\Delta S^o > 0$, hydrophobic forces dominate, while van der Waals forces and hydrogen bonding dominate the process when $\Delta H^o < 0$ and $\Delta S^o < 0$. Electrostatic forces are considered the main forces when $\Delta H^o < 0$ and $\Delta S^o > 0$. In case of slight temperature differences, Van't Hoff equation can be utilized for determining ΔH^o and ΔS^o[29,30].

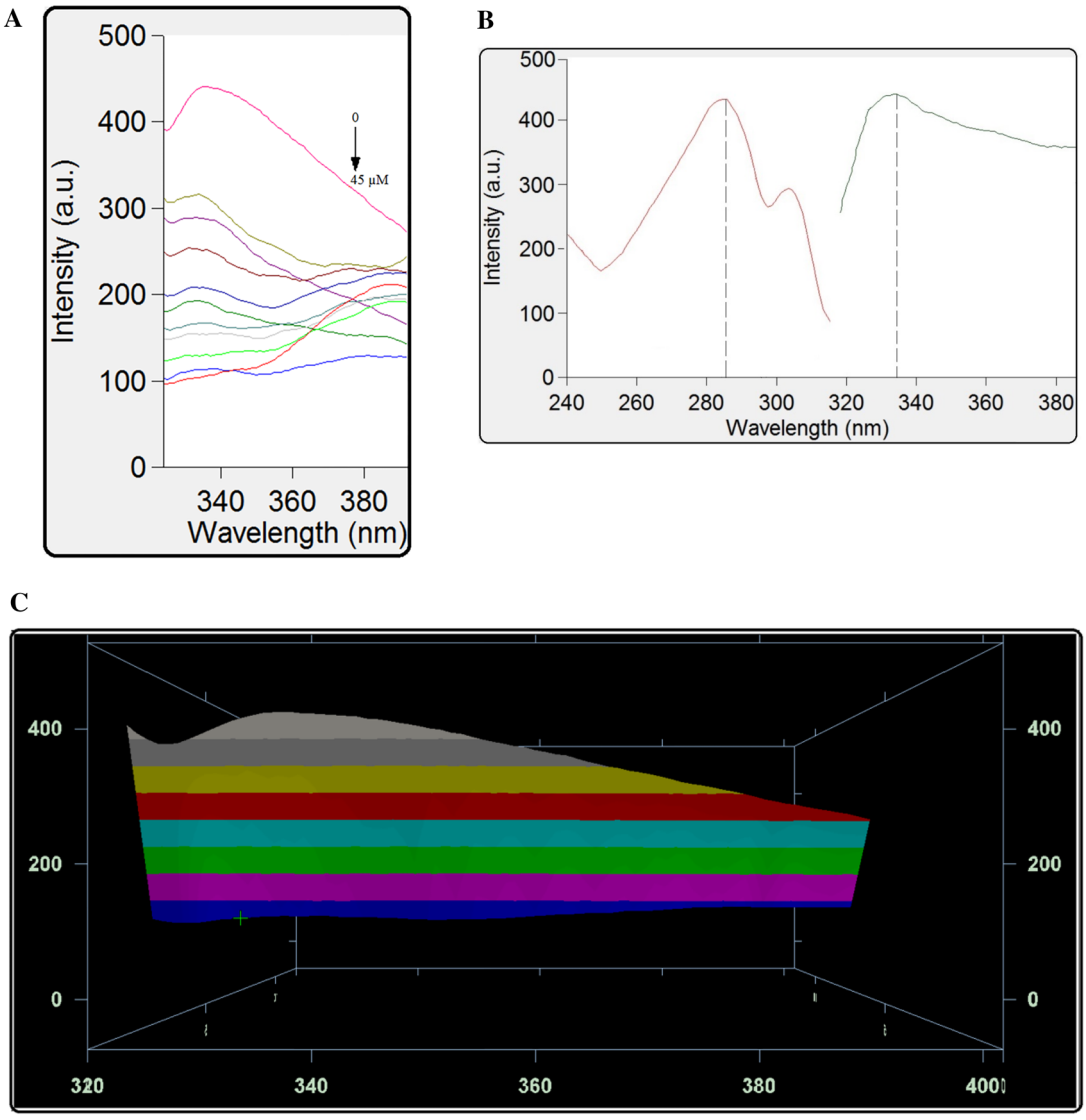

Figure 3. (**A**) Fluorescence spectra of BSA (40 μM) in presence of MBZ (4, 5, 10, 15, 20, 25, 30, 35, 40, 45 μM) at 298 K and pH 7.4. (**B**) Excitation (red curve) and emission (green curve) spectra for BSA 40 μM at 298 K and pH 7.4. (λ_{em}) = 338 nm and (λ_{ex}) = 285 nm. (**C**) 3D fluorescence spectra of BSA (40 μM) in presence of MBZ (4, 5, 10, 15, 20, 25, 30, 35, 40, 45 μM) at 298 K and pH 7.4.

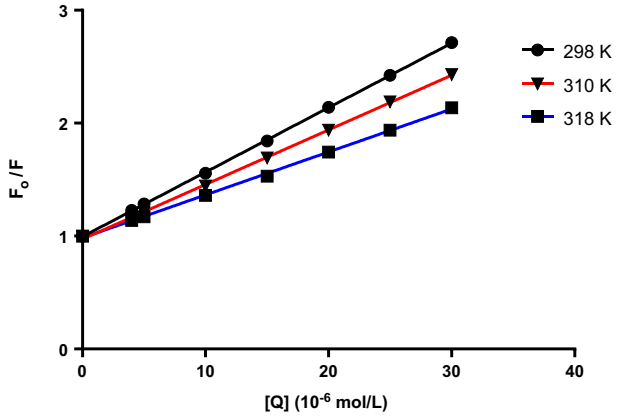

Figure 4. Stern–Volmer plots for BSA-MBZ system at various temperatures.

T (K)	K_{sv} (10^4 L mol^{-1})	kq (10^{12} L mol^{-1} s^{-1})	R^2	SD	%Error
298	5.657	5.657	0.9999	0.923	0.413
310	4.483	4.483	0.9994	1.232	0.551
318	3.623	3.623	0.9992	1.647	0.737

Table 1. MBZ-BSA interaction parameters at various temperatures.

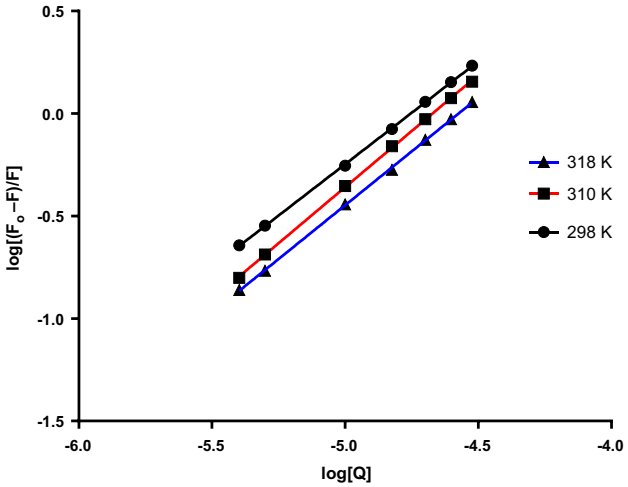

Figure 5. Plots of log (F_o–F)/F versus Log [Q] at three temperature settings.

T (K)	K (L mol^{-1})	n	R^2
298	5.67×10^4	1.003	0.9999
310	4.48×10^4	1.091	0.9997
318	3.76×10^4	1.049	0.9995

Table 2. MBZ-BSA complex binding characteristics at different temperatures.

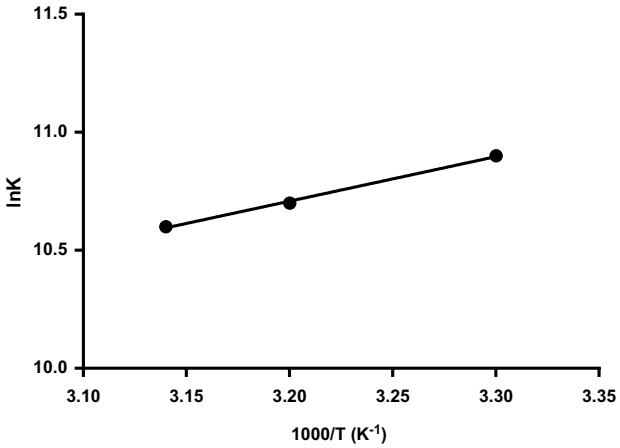

Figure 6. Van't Hoff plot for BSA- MBZ binding.

$$\ln K = -\frac{\Delta H^{\circ}}{RT} + \frac{\Delta S^{\circ}}{R} \tag{4}$$

where R is the gas constant and K_b is the binding constant at temperature T.

T (K)	ΔH° (kJ/mol)	ΔG° (kJ/mol)	ΔS° (J mol^{-1} K^{-1})	R^2
298	158.51	−31.83	638.75	0.9978
310		−39.49		
318		−44.61		

Table 3. Thermodynamic parameters of MBZ-BSA Interaction at pH 7.4.

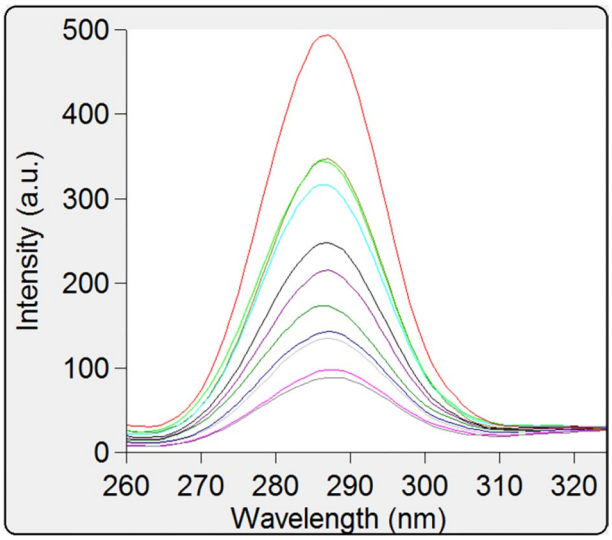

Figure 7. Synchronous fluorescence spectra of BSA (40 μM) at Δλ 15 nm in existence of MBZ (4, 5, 10, 15, 20, 25, 30, 35, 40, 45 μM).

A straight line is obtained by plotting ln K_b versus 1/ T. The resulting slope represents the enthalpy change (ΔH°), whereas the intercept represents the entropy change (ΔS°) (Fig. 6). The following equation can be used to calculate free energy change (ΔG°):

$$\Delta G^{\circ} = \Delta H^{\circ} - T\Delta S^{\circ} \tag{5}$$

As presented in Table 3, the negative free energy change (ΔG°) and the positive entropy change (ΔS°) reveal the spontaneous binding of MBZ-BSA complex. Furthermore, the main force in this reaction is the hydrophobic interaction. An endothermic reaction is revealed by associating the positive value of enthalpy change (ΔH°) and the increasing K values with the three different temperatures.

Synchronous fluorescence spectra of BSA. The synchronous spectrofluorimetric approach has many benefits: spectral simplicity, sensitivity, spectral bandwidth, as well as minimizing and preventing various disturbing effects. It is highly beneficial to accomplish the emission wavelength shift in order to investigate the protein's microenvironment[31]. In BSA, Trp and Tyr residues are revealed by the use of synchronous fluorescence spectra at wavelength intervals (Δλ) of 60 nm and 15 nm, respectively. It is further displayed in the synchronous fluorescence spectra of BSA at Δλ = 15 nm (Fig. 7) and at Δλ = 60 nm (Fig. 8) with different MBZ concentrations. In Fig. 7, at Δλ 15 nm, it was revealed that the maximum emission range for the studied concentrations remained unchanged, while at Δλ 60 nm, a minor blue shift (277–274 nm) was noticed as illustrated in Fig. 8. The polarity surrounding tryptophan residues was observed to be attenuated, suggesting that it occurred in a hydrophobic environment. Therefore, the conformation of BSA after binding with MBZ is suggested by the observed spectral change[32].

Site probe studies. BSA is composed of 3 domains: I, II, and III, with each domain, further subdivided into two subdomains A and B[3,33]. An investigation of site marker measurements was conducted to determine the MBZ binding site in BSA. According to Sudlow et al.[34], drugs bind to albumin at sites I or II, which are situated inside the hydrophobic regions of subdomains IIA and IIIA, respectively. Indomethacin binds to site I and diazepam binds to site II[35,36]. For calculation of the binding parameters resulting from the impact of both site markers on MBZ-BSA interaction, the Stern–Volmer equation was applied and the plot is shown in Fig. 9. The binding constants of the interaction between MBZ and BSA were calculated in the presence of the two site markers as shown in Table 4. Noticeably, MBZ binding with BSA is weakened in the presence of indomethacin.

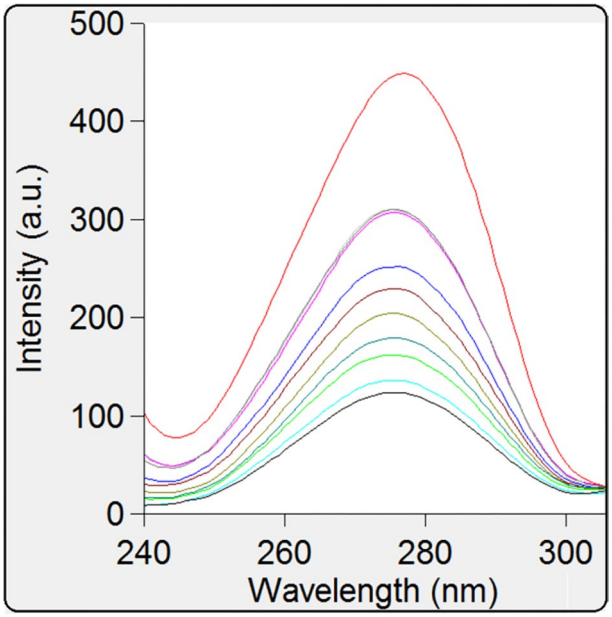

Figure 8. Synchronous fluorescence spectra of BSA (40 μM) at Δλ 60 nm in existence of MBZ (4, 5, 10, 15, 20, 25, 30, 35, 40, 45 μM).

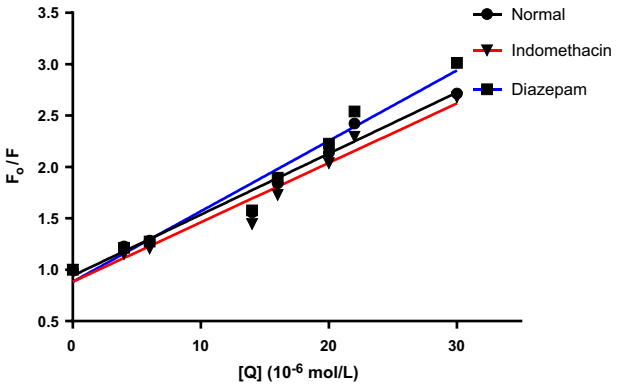

Figure 9. Stern–Volmer plots for BSA quenching by MBZ before and after adding site markers.

Site marker	K_{sv} (10^4 L mol^{-1})	kq (10^{12} L mol^{-1} s^{-1})	SD	%Error
BSA + MBZ	5.657	5.657	0.923	0.413
BSA + MBZ + IND	4.743	4.743	1.017	0.455
BSA + MBZ + DIA	5.94	5.94	0.908	0.406

Table 4. Stern volmer quenching constants and bimolecular quenching rate constants for MBZ- BSA interaction in presence of site markers.

However, the binding constant remained unchanged upon adding diazepam. Hence, it may be deduced that MBZ-BSA binding occurs at the site I of subdomain IIA. There is an agreement between these outcomes and the results of the molecular docking technique presented in "Molecular Docking"section.

FT-IR spectroscopy. FT-IR spectroscopy is effective for studying protein dynamics and secondary structures[37]. Confirmation of the interaction between MBZ and BSA is revealed by FT-IR spectra in Fig. 10. Amide bands are the main constituent of the protein's infrared spectra, as they cause many peptide moiety vibrations. The amides I and II peaks, which occur in the region of 1600–1700 cm^{-1} and 1500–1600 cm^{-1}, respectively, are often employed in secondary protein structure studies. The amide I band is more susceptible to alterations than the amide II band, which makes it useful for examining the protein's secondary structure. The amide I

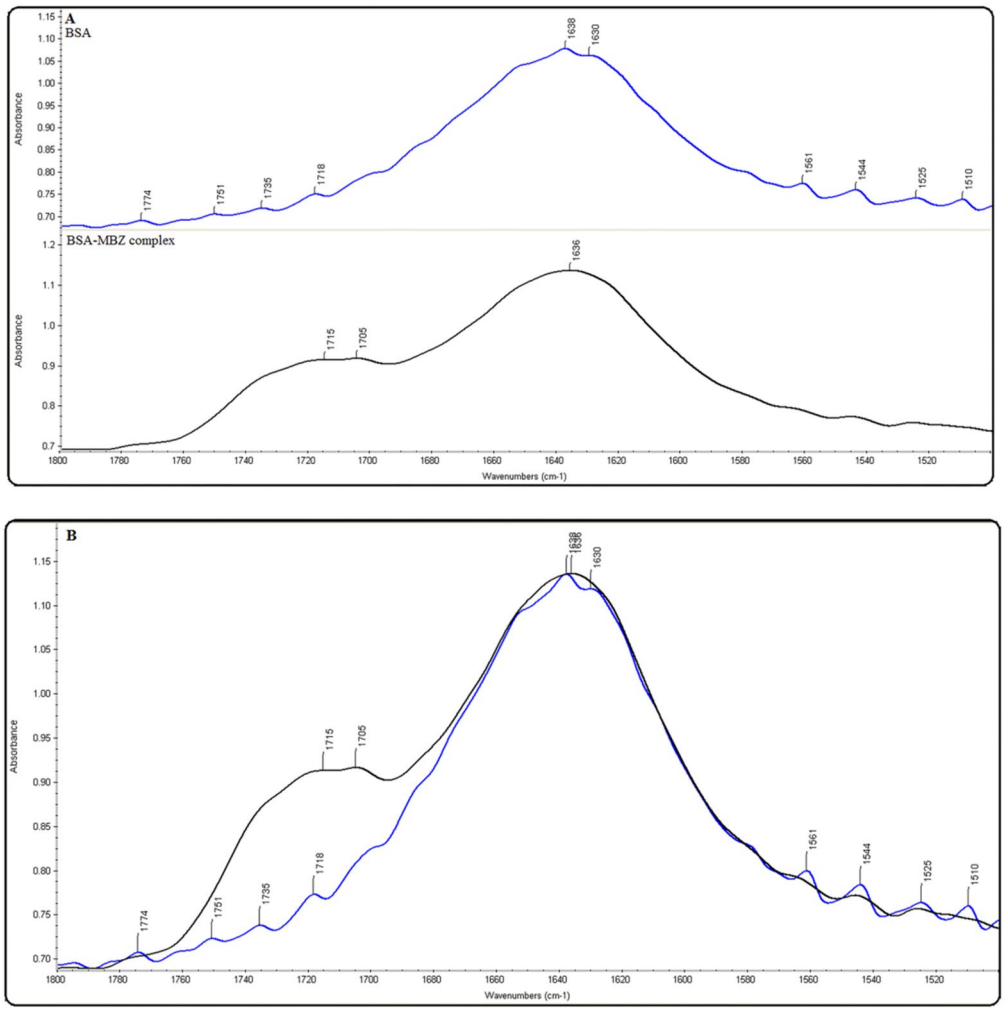

Figure 10. Free BSA and BSA-MBZ complex FTIR spectra at 298 K at pH 7.4.

peak location was shifted from 1638 to 1636 cm^{-1} after the MBZ reaction, suggesting that the secondary protein structure alters during MBZ-BSA interaction[38].

Fluorescence resonance energy transfer (FRET) between MBZ and BSA. FRET is a phenomenon that involves transferring non-radiative energy along with the distance between a donor molecule (BSA) and an acceptor molecule (MBZ). Resonance takes place in a distant-dependent manner through dipole–dipole coupling between the two fluorophores, in absence of molecular collision or thermal energy conversion. The non-radiative energy transfer theory proposed by Förster states that many factors have an influence on FRET[39]:

1. As illustrated in Fig. 11, there is an overlapping between the donor's emission spectra and the acceptor's absorption spectrum.
2. The magnitude of this overlap is represented by the spectral overlap integral (J).
3. Both the acceptor and donor molecules should have parallel transition dipole orientations.

To determine the efficiency of energy transfer (E), the following formula was applied:

$$E = 1 - \frac{F}{F_o} = \frac{R_o^6}{R_0^6 + r^6} \tag{6}$$

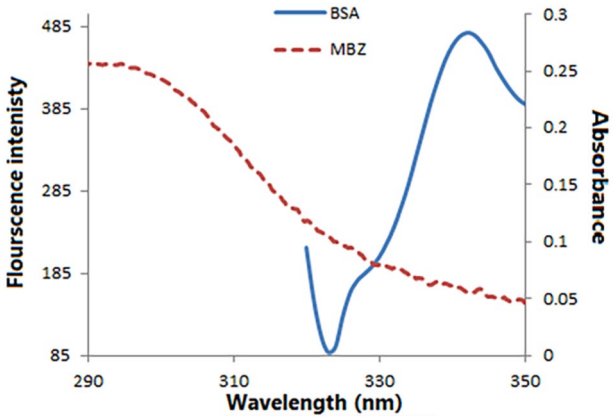

Figure 11. Spectral overlap between the BSA fluorescence emission spectrum (40 μM) and the absorption spectrum of MBZ (15 μM) at 298 K and pH 7.4.

where F_o and F represent BSA fluorescence intensity in absence and presence of MBZ, respectively. r signifies the distance between the BSA and the MBZ. R_o is the Förster distance where the energy transfer is 50% efficient.

Calculation of the value of R_o was obtained from Eq. (7):

$$R_o^6 = 8.8 \times 10^{-25} k^2 N^{-4} \Phi J \tag{7}$$

where k^2 is the dipole angular orientation of each molecule, N is the refractive index of the medium, Φ is the fluorescence quantum yield of the donor and J is the spectral overlap integral of the fluorescence emission spectrum of the donor and the absorption spectrum of the acceptor and was assessed by applying in the Eq. (8):

$$J = \frac{\int F(\lambda)\varepsilon(\lambda)\lambda^4 \Delta\lambda}{\int F(\lambda)\Delta\lambda} \tag{8}$$

where F (λ) is the fluorescence intensity of the fluorescent donor of wavelength λ. (λ) is the molar absorption coefficient of the acceptor at wavelength λ.

In this study, $k^2 = 2/3$. $N = 1.336$ and $\Phi = 0.15$. The spectral overlap integral (J) is determined over the range of 300–450 nm. The values of $J = 8.69 \times 10^{-16}$ cm^3 L mol^{-1}[40], $E = 0.42$, $R_o = 1.70$ nm and $r = 1.79$ nm can be computed from Eqs. (6) – (8). The average distance between BSA and MBZ is less than 8 nm suggesting that the energy transfer occurs[41].

Molecular docking. A useful simulation tool used in evaluating the nature of the drug-protein binding is Molecular docking. It was used to validate our data obtained about MBZ binding affinity and interactions at its binding site in BSA. Results are obtained from this technique, confirming the previously reported studies of the site marker displacement, i.e., the binding of MBZ with BSA at the site I of subdomain IIA (Fig. 12A,B). The configuration of MBZ was recorded after binding with BSA, revealing binding energy of – 6.9 kcal mol^{-1}. This MBZ conformer is located within the active site residues Arg194, Arg198, Ala290, Trp213, Arg217, Leu259, Leu237, lys221, Ile289, Ile263 and Asp450 (Fig. 12A,B). Furthermore, it was shown that MBZ formed hydrophobic interaction with BSA through residue Trp213. Results from molecular modeling correlate with the previous experimental results proving the occurrence of MBZ-BSA binding through hydrophobic interaction.

Conclusion

In this proposed study, an evaluation of the MBZ-BSA binding interaction is established under physiological conditions with the use of multi-spectroscopic and molecular docking approaches. Intensive research has been conducted using a variety of techniques. MBZ-BSA binding was found to be static quenching. The thermodynamic parameters for MBZ-BSA interaction were also determined. The binding of MBZ-BSA was a spontaneous endothermic process, with hydrophobic interaction being the dominating factor in the process. In accordance with the site marker technique which was confirmed by molecular docking studies, MBZ-BSA binding occurs at site I in subdomain IIA. This study provides valuable insights into a better understanding of the pharmacokinetic profile of MBZ. The data presented in this work might help in understanding the molecular mechanisms underlying the harmful side effects of MBZ, thereby improving its pharmacological and clinical efficacy. The results proved the binding relationship between MBZ and BSA as well as the ease of transportation and elimination, suggesting recommendations for further studies and research. This study can provide experimental evidence of MBZ toxicity and supply basic data for its safe use.

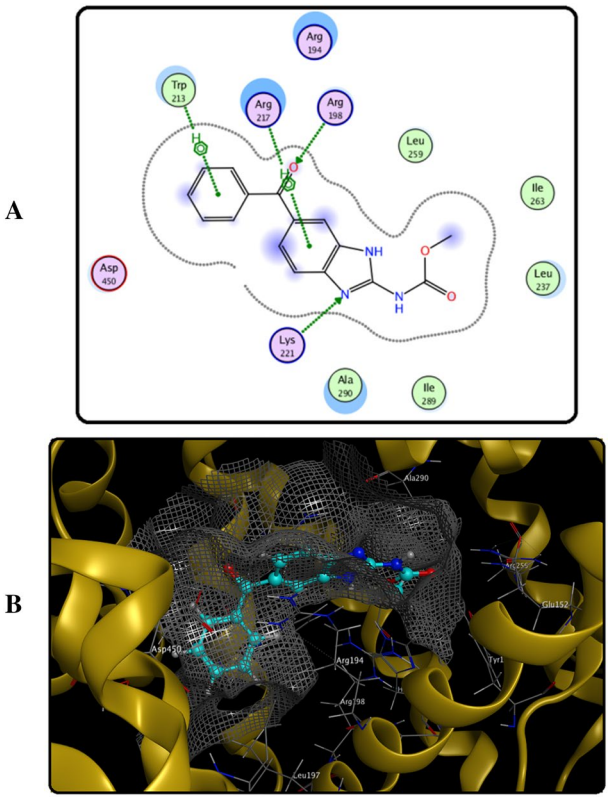

Figure 12. (**A**) Diagram for the amino acid residues incorporated in MBZ-BSA interaction within the binding pocket of BSA site 1, (**B**) 3D structure of the binding interaction between MBZ-BSA.

Data availability

All data generated or analyzed during this study are included in this published article.

Received: 16 April 2022; Accepted: 28 June 2022
Published online: 08 July 2022

References

1. Müller, W. E. & Wollert, U. Human serum albumin as a "silent receptor" for drugs and endogenous substances. *Pharmacology* **19**(2), 59–67 (1979).
2. Ketrat, S., Japrung, D. & Pongprayoon, P. Exploring how structural and dynamic properties of bovine and canine serum albumins differ from human serum albumin. *J. Mol. Graph. Model.* **98**, 107601 (2020).
3. Carter, D. C. & Ho, J. X. Structure of serum albumin. *Adv. Protein Chem.* **45**, 153–203 (1994).
4. Huang, B. X., Kim, H.-Y. & Dass, C. Probing three-dimensional structure of bovine serum albumin by chemical cross-linking and mass spectrometry. *J. Am. Soc. Mass Spectrom.* **15**(8), 1237–1247 (2004).
5. Xu, H., Liu, Q., Zuo, Y., Bi, Y. & Gao, S. Spectroscopic studies on the interaction of vitamin C with bovine serum albumin. *J. Sol. Chem.* **38**(1), 15–25 (2009).
6. Bertucci, C. & Domenici, E. Reversible and covalent binding of drugs to human serum albumin: Methodological approaches and physiological relevance. *Curr. Med. Chem.* **9**(15), 1463–1481 (2002).
7. Tesseromatis, C. & Alevizou, A. The role of the protein-binding on the mode of drug action as well the interactions with other drugs. *Eur. J. Drug Metab. Pharmacokinet.* **33**(4), 225–230 (2008).
8. Ali, M. S. & Al-Lohedan, H. A. Deciphering the interaction of procaine with bovine serum albumin and elucidation of binding site: A multi spectroscopic and molecular docking study. *J. Mol. Liq.* **236**, 232–240 (2017).
9. Buckingham, R. *Martindale: The Complete Drug Reference Brayfield Aliso* 148–149 (Pharma Press, 2020).
10. Guerini, A. E. *et al.* Mebendazole as a candidate for drug repurposing in oncology: An extensive review of current literature. *Cancers* **11**(9), 1284 (2019).
11. Wishart, D. S. *et al.* DrugBank 5.0: A major update to the DrugBank database for 2018. *Nucleic Acids Res.* **46**(D1), D1074–D1082 (2018).
12. Lakowicz, J. R. *Principles of Fluorescence Spectroscopy* 11 (Springer, 2013).
13. Bujacz, A. Structures of bovine, equine and leporine serum albumin. *Acta Crystallogr. D Biol. Crystallogr.* **68**(Pt 10), 1278–1289 (2012).
14. Yan, F., Liu, G., Chen, T., Fu, X. & Niu, M. M. Structure-based virtual screening and biological evaluation of peptide inhibitors for polo-box domain. *Molecules* **25**(1), 107 (2019).
15. Pan, X., Qin, P., Liu, R. & Wang, J. Characterizing the Interaction between tartrazine and two serum albumins by a hybrid spectroscopic approach. *J. Agric. Food Chem.* **59**(12), 6650–6656 (2011).
16. Abdullah, S. M. S., Fatma, S., Rabbani, G. & Ashraf, J. M. A spectroscopic and molecular docking approach on the binding of tinzaparin sodium with human serum albumin. *J. Mol. Struct.* **1127**, 283–288 (2017).

17. Molina-Bolívar, J. A., Galisteo-González, F., Carnero-Ruiz, C., Medina-O' Donnell, M. & Parra, A. Spectroscopic investigation on the interaction of maslinic acid with bovine serum albumin. *Luminescence* **156**, 141–149 (2014).
18. Mocz, G. & Ross, J. A. Fluorescence Techniques in Analysis of Protein-Ligand Interactions. In *Protein-Ligand Interactions: Methods and Applications* (eds Williams, M. A. & Daviter, T.) 169–210 (Humana Press, 2013).
19. Suryawanshi, V. D., Walekar, L. S., Gore, A. H., Anbhule, P. V. & Kolekar, G. B. Spectroscopic analysis on the binding interaction of biologically active pyrimidine derivative with bovine serum albumin. *J. Pharm. Anal.* **6**(1), 56–63 (2016).
20. Wang, B. L., Pan, D. Q., Zhou, K. L., Lou, Y. Y. & Shi, J. H. Multi-spectroscopic approaches and molecular simulation research of the intermolecular interaction between the angiotensin-converting enzyme inhibitor (ACE inhibitor) benazepril and bovine serum albumin (BSA). *Spectrochim. Acta A Mol Biomol. Spectrosc.* **212**, 15–24 (2019).
21. Paramaguru, G., Kathiravan, A., Selvaraj, S., Venuvanalingam, P. & Renganathan, R. Interaction of anthraquinone dyes with lysozyme: Evidences from spectroscopic and docking studies. *J Hazard Mater.* **175**(1–3), 985–991 (2010).
22. Zhao, X., Liu, R., Chi, Z., Teng, Y. & Qin, P. New insights into the behavior of bovine serum albumin adsorbed onto carbon nanotubes: Comprehensive spectroscopic studies. *J. Phys. Chem. B.* **114**(16), 5625–5631 (2010).
23. Hu, Y. J., Ou-Yang, Y., Dai, C. M., Liu, Y. & Xiao, X. H. Binding of berberine to bovine serum albumin: Spectroscopic approach. *Mol. Biol. Rep.* **37**(8), 3827–3832 (2010).
24. Lakowicz, J. R. & Weber, G. Quenching of fluorescence by oxygen: A probe for structural fluctuations in macromolecules. *Biochemistry* **12**(21), 4161–4170 (1973).
25. Hu, Y.-J., Liu, Y., Zhao, R.-M., Dong, J.-X. & Qu, S.-S. Spectroscopic studies on the interaction between methylene blue and bovine serum albumin. *J. Photochem. Photobiol. A Chem.* **179**(3), 324–329 (2006).
26. Macii, F. & Biver, T. Spectrofluorimetric analysis of the binding of a target molecule to serum albumin: Tricky aspects and tips. *J. Inorg. Biochem.* **216**, 111305 (2021).
27. Wei, X. F. & Liu, H. Z. The interaction between Triton X-100 and bovine serum albumin. *Chin. J. Anal. Chem.* **28**, 699–701 (2000).
28. Klotz, I. M. Physiochemical aspects of drug-protein interactions: A general perspective. *Ann. NY Acad. Sci.* **226**, 18–35 (1973).
29. Ross, P. D. & Subramanian, S. Thermodynamics of protein association reactions: Forces contributing to stability. *Biochemistry* **20**(11), 3096–3102 (1981).
30. Otagiri, M. A molecular functional study on the interactions of drugs with plasma proteins. *Drug Metab. Pharmacokinet.* **20**(5), 309–323 (2005).
31. Abdelhameed, A. S. *et al.* Fluorescence spectroscopic and molecular docking studies of the binding interaction between the new anaplastic lymphoma kinase inhibitor crizotinib and bovine serum albumin. *Spectrochim. Acta A Mol. Biomol. Spectrosc.* **171**, 174–182 (2017).
32. Pawar, S. K. & Jaldappagari, S. Interaction of repaglinide with bovine serum albumin: Spectroscopic and molecular docking approaches. *J. Pharm. Anal.* **9**(4), 274–283 (2019).
33. Peters, T. The Albumin Molecule: Its Structure and Chemical Properties. In *All About Albumin* (ed. Peters, T.) 9–II (Academic Press, 1995).
34. Sudlow, G., Birkett, D. J. & Wade, D. N. Further characterization of specific drug binding sites on human serum albumin. *Mol. Pharmacol.* **12**(6), 1052–1061 (1976).
35. Cheng, X.-X., Lui, Y., Zhou, B., Xiao, X.-H. & Liu, Y. Probing the binding sites and the effect of berbamine on the structure of bovine serum albumin. *Spectrochim. Acta A Mol. Biomol. Spectrosc.* **72**(5), 922–928 (2009).
36. Zhang, Y.-Z., Dai, J., Xiang, X., Li, W.-W. & Liu, Y. Studies on the interaction between benzidine and bovine serum albumin by spectroscopic methods. *Mol. Biol. Rep.* **37**(3), 1541–1549 (2010).
37. Harding, S. E., Chowdhry, B. Z. Protein-ligand interactions, structure and spectroscopy: A practical approach: Practical Approach (Paperback); (2001).
38. Zhang, Y., Yang, Y. & Guo, T. Genipin-crosslinked hydrophobical chitosan microspheres and their interactions with bovine serum albumin. *Carbohydr. Polym.* **83**(4), 2016–2021 (2011).
39. Naik, P. N., Chimatadar, S. A. & Nandibewoor, S. T. Interaction between a potent corticosteroid drug-dexamethasone with bovine serum albumin and human serum albumin: A fluorescence quenching and fourier transformation infrared spectroscopy study. *J. Photochem. Photobiol. B* **100**(3), 147–159 (2010).
40. Banerjee, P., Ghosh, S., Sarkar, A. & Bhattacharya, S. C. Fluorescence resonance energy transfer: A promising tool for investigation of the interaction between 1-anthracene sulphonate and serum albumins. *Luminescence* **131**(2), 316–321 (2011).
41. Wang, B.-L., Kou, S.-B., Lin, Z.-Y. & Shi, J.-H. Investigation on the binding behavior between BSA and lenvatinib with the help of various spectroscopic and in silico methods. *J. Mol. Struct.* **1204**, 127521 (2020).

Acknowledgements

The authors would like to thank the Alexander von Humboldt Foundation, Bonn,Germany for donating the instrument used in this study (Spectrofluorometer) to one of the authors (FB).

Author contributions

All authors have made substantial contributions to material submitted; All authors conceived and designed the study. R.N.ElG. conducted the experiments, analyzed the data and wrote the paper. M.E.A.H. studied the molecular docking part. All authors have read and approved the final manuscript.

Funding

Open access funding provided by The Science, Technology & Innovation Funding Authority (STDF) in cooperation with The Egyptian Knowledge Bank (EKB).

Competing interests

The authors declare no competing interests.

Additional information

Correspondence and requests for materials should be addressed to R.N.E.G.

Reprints and permissions information is available at www.nature.com/reprints.

Publisher's note Springer Nature remains neutral with regard to jurisdictional claims in published maps and institutional affiliations.

Open Access This article is licensed under a Creative Commons Attribution 4.0 International License, which permits use, sharing, adaptation, distribution and reproduction in any medium or format, as long as you give appropriate credit to the original author(s) and the source, provide a link to the Creative Commons licence, and indicate if changes were made. The images or other third party material in this article are included in the article's Creative Commons licence, unless indicated otherwise in a credit line to the material. If material is not included in the article's Creative Commons licence and your intended use is not permitted by statutory regulation or exceeds the permitted use, you will need to obtain permission directly from the copyright holder. To view a copy of this licence, visit http://creativecommons.org/licenses/by/4.0/.

© The Author(s) 2022